

ARCHIVAL REPORT

Disrupted Functional Brain Connectome in Individuals at Risk for Alzheimer's Disease

Jinhui Wang, Xinian Zuo, Zhengjia Dai, Mingrui Xia, Zhilian Zhao, Xiaoling Zhao, Jianping Jia, Ying Han, and Yong He

Background: Alzheimer's disease disrupts the topological architecture of whole-brain connectivity (i.e., the connectome); however, whether this disruption is present in amnesic mild cognitive impairment (aMCI), the prodromal stage of Alzheimer's disease, remains largely unknown.

Methods: We employed resting-state functional magnetic resonance imaging and graph theory approaches to systematically investigate the topological organization of the functional connectome of 37 patients with aMCI and 47 healthy control subjects. Frequency-dependent brain networks were derived from wavelet-based correlations of both high- and low-resolution parcellation units.

Results: In the frequency interval .031–.063 Hz, the aMCI patients showed an overall decreased functional connectivity of their brain connectome compared with control subjects. Further graph theory analyses of this frequency band revealed an increased path length of the connectome in the aMCI group. Moreover, the disease targeted several key nodes predominantly in the default-mode regions and key links primarily in the intramodule connections within the default-mode network and the intermodule connections among different functional systems. Intriguingly, the topological aberrations correlated with the patients' memory performance and differentiated individuals with aMCI from healthy elderly individuals with a sensitivity of 86.5% and a specificity of 85.1%. Finally, we demonstrated a high reproducibility of our findings across different large-scale parcellation schemes and validated the test-retest reliability of our network-based approaches.

Conclusions: This study demonstrates a disruption of whole-brain topological organization of the functional connectome in aMCI. Our finding provides novel insights into the pathophysiological mechanism of aMCI and highlights the potential for using connectome-based metrics as a disease biomarker.

Key Words: Connectivity, connectomics, default-mode, MCI, modularity, small-world

Alzheimer's disease (AD) is a progressive, neurodegenerative disease characterized by a decline in cognitive and memory functions likely caused by aberrant neuronal circuitry (1–3). Amnesic mild cognitive impairment (aMCI), a transition state between normal aging and AD, has a high risk of progressing to AD (4). Numerous studies have reported that the brains of patients with aMCI have impaired structural integrity (5,6) and functional connectivity (7–10). However, whether aMCI patients also exhibit a disrupted topological organization in their whole-brain networks remains largely unknown.

Recent studies have suggested that human whole-brain structural and functional networks (i.e., the connectome [11,12]) can be constructed using multimodal neuroimaging data and that their topological organization can be characterized quantitatively using various graph theory metrics (13–15). With these metrics, many nontrivial organizational principles, including small-worldness, modularity, and highly connected hubs, have been observed in the human brain connectome. Moreover, these network properties are disrupted in many neuropsychiatric disorders (13,16–18). These studies have accelerated the process of mapping the human con-

nectome in healthy and diseased states. Specifically, in patients with AD, several research groups have reported topological alterations in the whole-brain connectome, including a loss of small-worldness and a redistribution of hubs (19–23). With respect to aMCI, only two studies have explored the topological organization of the whole-brain connectome. Using structural magnetic resonance imaging, Yao *et al.* (24) found no differences in the topology of cortical-thickness networks between patients with aMCI and healthy control subjects. However, using magnetoencephalography data, Buldu *et al.* (25) reported reorganization of the functional connectome in aMCI patients during a memory task.

Here, we employed resting-state functional magnetic resonance imaging (R-fMRI) to investigate the topological changes in the functional connectome in patients with aMCI. R-fMRI measures intrinsic or spontaneous neuronal activity of the brain (26,27) and has been applied to reveal aMCI-related breakdowns in functional brain synchronization (7,9,28). The current study focuses exclusively on the topological architecture of the intrinsic functional brain connectome in aMCI. Specifically, we sought to determine whether aMCI disrupts the topological organization of the whole-brain functional network and, if so, whether those topological abnormalities are associated with individual clinical or behavioral variables. Furthermore, we examined whether these abnormalities differentiated patients with aMCI from healthy elderly individuals.

Methods and Materials

Participants

Eighty-four right-handed participants, comprising 37 patients with aMCI (17 men and 20 women) and 47 sex-, age-, and education-matched healthy control subjects (HC: 20 men and 27 women), participated in this study. The patients were recruited from the memory clinic of the neurology department of Xuanwu Hospital, Capital Medical University, Beijing, China. The control subjects were recruited from the local community using advertisements. At the time of the study, none of the patients had ever been treated with

From the State Key Laboratory of Cognitive Neuroscience and Learning (JW, ZD, MX, YHe), Beijing Normal University; Laboratory for Functional Connectome and Development (XZu), Key Laboratory of Behavioral Science, Magnetic Resonance Imaging Research Center, Institute of Psychology, Chinese Academy of Sciences; and Departments of Radiology (ZZ) and Neurology (XZh, JJ, YHa), Xuanwu Hospital, Capital Medical University, Beijing, China.

Address correspondence to Yong He, Ph.D., Beijing Normal University, State Key Laboratory of Cognitive Neuroscience and Learning, No 19 Xinjiekouwai Street, Haidian District, Beijing 100875, China; E-mail: yong.he@bnu.edu.cn.

Received Jan 12, 2012; revised Mar 15, 2012; accepted Mar 26, 2012.

Table 1. Demographics and Clinical Characteristics of the Participants

	HC (<i>n</i> = 47)	aMCI (<i>n</i> = 37)	<i>p</i> Value
Gender (Male/ Female)	20/27	17/20	.756 ^a
Age (Years)	50–79 (63.4 ± 7.7)	41–79 (66.8 ± 9.4)	.184 ^b
Education (Years)	0–22 (11.4 ± 5.0)	0–20 (9.8 ± 4.2)	.136 ^b
MMSE	20–30 (28.5 ± 2.0)	16–30 (24.7 ± 3.5)	<10 ^{−7b}
CDT	1–3 (2.8 ± .6)	1–3 (2.1 ± .8)	<10 ^{−4b}
CDR	0	.5	—
AVLT-Immediate Recall	6–14.7 (8.8 ± 2.0)	2.7–10.7 (5.7 ± 1.9)	<10 ^{−9b}
AVLT-Delayed Recall	4–15 (9.8 ± 2.8)	0–14 (5.1 ± 3.3)	<10 ^{−9b}
AVLT-Recognition	3–15 (11.6 ± 2.7)	1–14 (8.8 ± 3.3)	<10 ^{−4b}

Data are presented as the range of minimum–maximum (mean ± SD). Notably, there were no outliers for any characteristics of both of the groups using the criterion of 2.5 interquartile ranges from lower/upper quartile values of the samples.

aMCI, amnesic mild cognitive impairment; AVLT, Auditory Verbal Learning Test; CDR, Clinical Dementia Rating Scale; CDT, Clock Drawing Test; HC, healthy control subjects; MMSE, Mini-Mental State Examination.

^aThe *p* value was obtained using a two-tail Pearson chi-square test.

^bThe *p* value was obtained using a two-sample two-tail *t* test.

specific medications, such as anti-acetylcholinesterase drugs. Diagnoses of aMCI were made by experienced neurologists using Petersen's criteria (4,29). The detailed inclusion and exclusion criteria are described in Supplement 1. Each participant was assessed using a standardized clinical evaluation protocol that included the Mini-Mental State Examination (MMSE) (30), the Clock Drawing Test (CDT), the Auditory Verbal Learning Test (AVLT) (31), and the Clinical Dementia Rating Scale (32). In Table 1, we present the detailed demographics and clinical characteristics of the participants. Datasets from a subset of the general population have been used to study local brain activity in patients with aMCI (33). This study was approved by the Medical Research Ethics Committee and Institutional Review Board of Xuanwu Hospital, and informed consent was obtained from each participant.

Data Acquisition

All participants were scanned using a 3.0 T Siemens Trio scanner (Erlangen, Germany) at Xuanwu Hospital, Capital Medical University, within a single session (Supplement 1). During the data acquisition, participants were asked to lie quietly in the scanner with their eyes closed. The scan lasted for 478 seconds in total and included 239 volumes for each participant.

Data Preprocessing

Data preprocessing was performed using the SPM8 package (<http://www.fil.ion.ucl.ac.uk/spm/software/SPM8/>; Wellcome Trust Center for Neuroimaging, University College London, United Kingdom; Supplement 1) and included the removal of the first five volumes, correction for time offsets between slices and head motion, spatial normalization to the Montreal Neurological Institute space, temporal high-pass filtering (cutoff frequency = .01 Hz), and regression of nuisance signals of six head-motion profiles. Given the controversy of removing the global signal in the preprocessing of R-fMRI data (34,35), we did not regress the global signal out (22,36,37). Notably, the head-motion profiles were matched between the aMCI and HC groups ($p > .248$ in any direction).

Network Construction

In this study, brain networks were constructed at the macroscale where nodes represented brain regions and edges represented

interregional resting-state functional connectivity (RSFC). To define network nodes, we divided the brain into 1024 regions of interest (ROIs) according to a high-resolution, randomly generated brain atlas (H-1024) (38). To measure interregional RSFC, we calculated the Pearson correlation between any pair of ROIs in the wavelet coefficients that were obtained by the maximal overlap discrete wavelet transform method (39). Here, we estimated RSFC in four wavelet scales (scale 1, .125–.250 Hz; scale 2, .063–.125 Hz; scale 3, .031–.063 Hz; and scale 4, .016–.031 Hz). To further de-noise spurious interregional correlations, only those correlations whose corresponding *p* values passed through a statistical threshold ($p < .05$, Bonferroni-corrected) were retained (40). Details on the network construction can be found in Supplement 1.

Network Analysis

For the constructed brain networks, we calculated both global and regional network metrics to characterize their overall architecture and regional nodal centrality, respectively. The global network metrics included small-world attributes (clustering coefficient, C^w and characteristic path length, L^w) (41) and modularity (Q_{\max}) (42) and their normalized versions using random networks (\tilde{C}^w , \tilde{L}^w , and \tilde{Q}_{\max}). Typically, a small-world network shows $\tilde{C}^w > 1$ and $\tilde{L}^w \approx 1$ (41) and a modular network shows $\tilde{Q}_{\max} > 1$. For regional network measures, we employed nodal strength (i.e., weighted degree centrality) among numerous nodal metrics (43) because of its high test-retest reliability (44). See Supplement 1 for the formulas and Rubinov and Sporns (45) for a recent review on the uses and interpretations of these network measures.

Statistical Analysis

Between-Group Differences. Between-group differences in topological attributes (both global and regional measures) were inferred by nonparametric permutation tests (21,46). Briefly, for each network metric, we initially calculated the between-group difference of the mean values. An empirical distribution of the difference was then obtained by randomly reallocating all of the values into two groups and recomputing the mean differences between the two randomized groups (10,000 permutations). The 95th percentile points of the empirical distribution were used as critical values in a one-tailed test of whether the observed group differences could occur by chance. To localize the specific pairs of regions in which the functional connectivity was altered in the aMCI patients, we used a network-based statistic (NBS) approach (47). In brief, a primary cluster-defining threshold was first used to identify suprathreshold connections, within which the size (i.e., number of edges) of any connected components was then determined. A corrected *p* value was calculated for each component using the null distribution of maximal connected component size, which was derived empirically using a nonparametric permutation approach (10,000 permutations). Notably, before the permutation tests, multiple linear regressions were applied to remove the effects of age and gender, the age-gender interaction, and education level (43,48–53). The details of the statistical analyses can be found in Supplement 1.

Relationships Between Network Measures and Clinical Variables. Multiple linear regressions were used to assess the relationships between network metrics and clinical variables (AVLT-immediate recall, AVLT-delayed recall, AVLT-recognition, and MMSE score) in the aMCI group. Age, gender, the age-gender interaction, and education level were also controlled.

Network Classification

We plotted the receiver operating characteristic curves to determine whether graph-based network metrics might serve as biomarkers for diagnosing aMCI. This analysis was performed using the

public MATLAB codes (<http://www.mathworks.com/matlabcentral/fileexchange/199500-roc-curve>; Giuseppe Cardillo, Naples, Italy; Supplement 1).

Validations: Reproducibility and Test-Retest Reliability

To validate the reproducibility of our results, we adopted four procedures as follows.

Preprocessing Choices. We explored the reproducibility of our results with and without regressing out white matter and cerebrospinal fluid signals.

Regional Parcellation Effects. We employed three low-resolution brain atlases (Table S1 in Supplement 1) to define network nodes, which allowed us to estimate the reproducibility of our findings against different parcellation schemes.

Network Types Effects. Besides the weighted network analysis, we also implemented binary network analyses to assess the stability of our findings.

Test-Retest Reliability. We used a public R-fMRI dataset at Neuroimaging Informatics Tools and Resources Clearinghouse (http://www.nitrc.org/projects/nyu_trt; New York University) to estimate the test-retest reliability of wavelet-based network metrics. Intraclass correlation (54) was used (for details, see Supplement 1).

Results

Demographic and Clinical Characteristics

There were no significant differences in age, gender, or years of education (all $p > .13$) between the aMCI and HC groups. However,

the aMCI group had significantly lower scores on the MMSE ($p < 10^{-7}$), CDT ($p < 10^{-4}$), AVLT-immediate recall ($p < 10^{-9}$), AVLT-delayed recall ($p < 10^{-9}$), and AVLT-recognition ($p < 10^{-4}$) than the HC group (Table 1).

Frequency-Specific Alterations in the Wavelet Correlation Matrix

For each thresholded wavelet correlation matrix, we calculated the total number of links, the mean correlation, and mean anatomical distance (defined as the Euclidean distance between stereotaxic coordinates of the centroids for two regions) for all significantly ($p < .05$, Bonferroni-corrected) existing connections. The aMCI networks had a significantly lower mean wavelet correlation ($p = .048$) and contained a higher proportion of short-range (anatomical distance < 45 mm) connections ($p = .046$) only in wavelet scale 3 (.031–.063 Hz). Additionally, trends toward fewer connections ($p = .080$), shorter mean anatomical distances ($p = .051$), and lower proportion of middle-range ($p = .058$) and long-range connections ($p = .058$) were also detected in the aMCI connectome (Figure 1). No significant between-group differences were detected in other frequency bands (all $p > .05$). Thus, the subsequent network topological analyses focused only on wavelet scale 3.

Global Topological Organization of the Functional Connectome

The whole-brain connectome of both the aMCI and HC groups exhibited typical features of small-world topology and modular

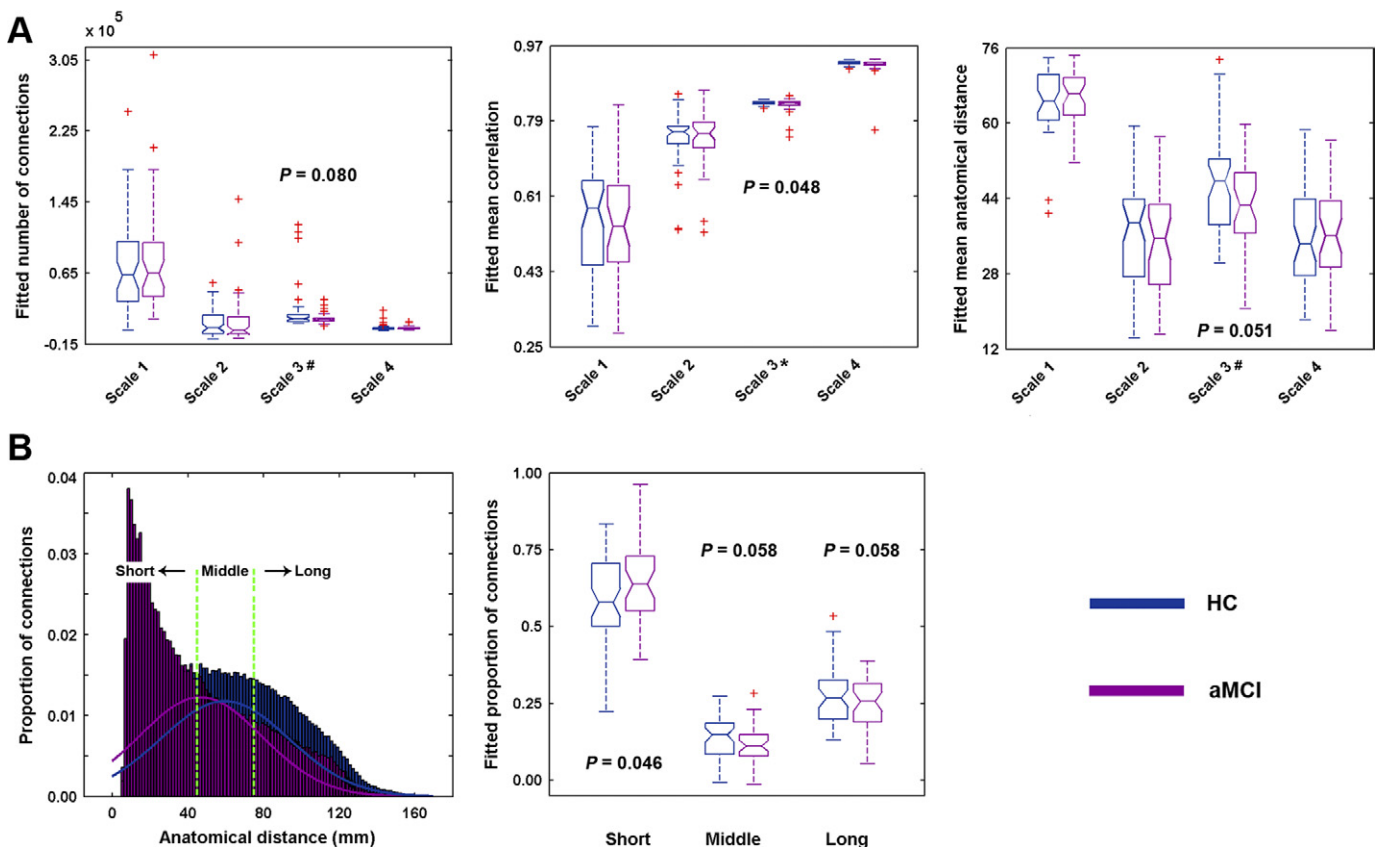


Figure 1. (A) Between-group differences in the number of connections (left), mean correlation (middle), and mean anatomical distance (right) of the functional networks and distribution of wavelet correlations with respect to bins of anatomical distance (B). In the specific wavelet scale 3 (.031–.063 Hz), the amnesic mild cognitive impairment (aMCI) patients exhibited fewer connections, lower mean correlation, and shorter mean anatomical distance. Further analysis revealed that aMCI targeted more middle- and long-distance connections (B). * $p < .05$; # $.05 \leq p \leq .10$. HC, healthy control subjects.

structure, i.e., compared with matched random networks, the functional brain networks had larger clustering coefficients, almost identical shortest path lengths, and larger modularity. Nevertheless, quantitative statistical analyses revealed significantly increased characteristic path lengths in the aMCI group (HC: 7.950 ± 5.236 ; aMCI: 14.506 ± 22.250 ; $p = .047$). Additionally, the aMCI group showed trends toward increased normalized characteristic path lengths (HC: $1.673 \pm .412$; aMCI: $1.928 \pm .694$; $p = .055$) and decreased modularity (HC: 3.129 ± 1.015 ; aMCI: $2.696 \pm .632$; $p = .084$) compared with the HC group.

Regional Topological Organization of the Functional Connectome

The mean nodal strength (across subjects) was distributed heterogeneously across the brain. In the HC group, the most highly connected regions were located predominantly in the posterior parietal and occipital cortices, such as the bilateral precuneus (PCUN), postcentral gyrus, superior parietal gyrus, cuneus, and calcarine fissure and surrounding cortex (Figure 2A). This pattern was highly preserved in the aMCI patients ($r = .834$, $p < 10^{-10}$, Figure 2B). Further between-group comparisons revealed that 27 brain

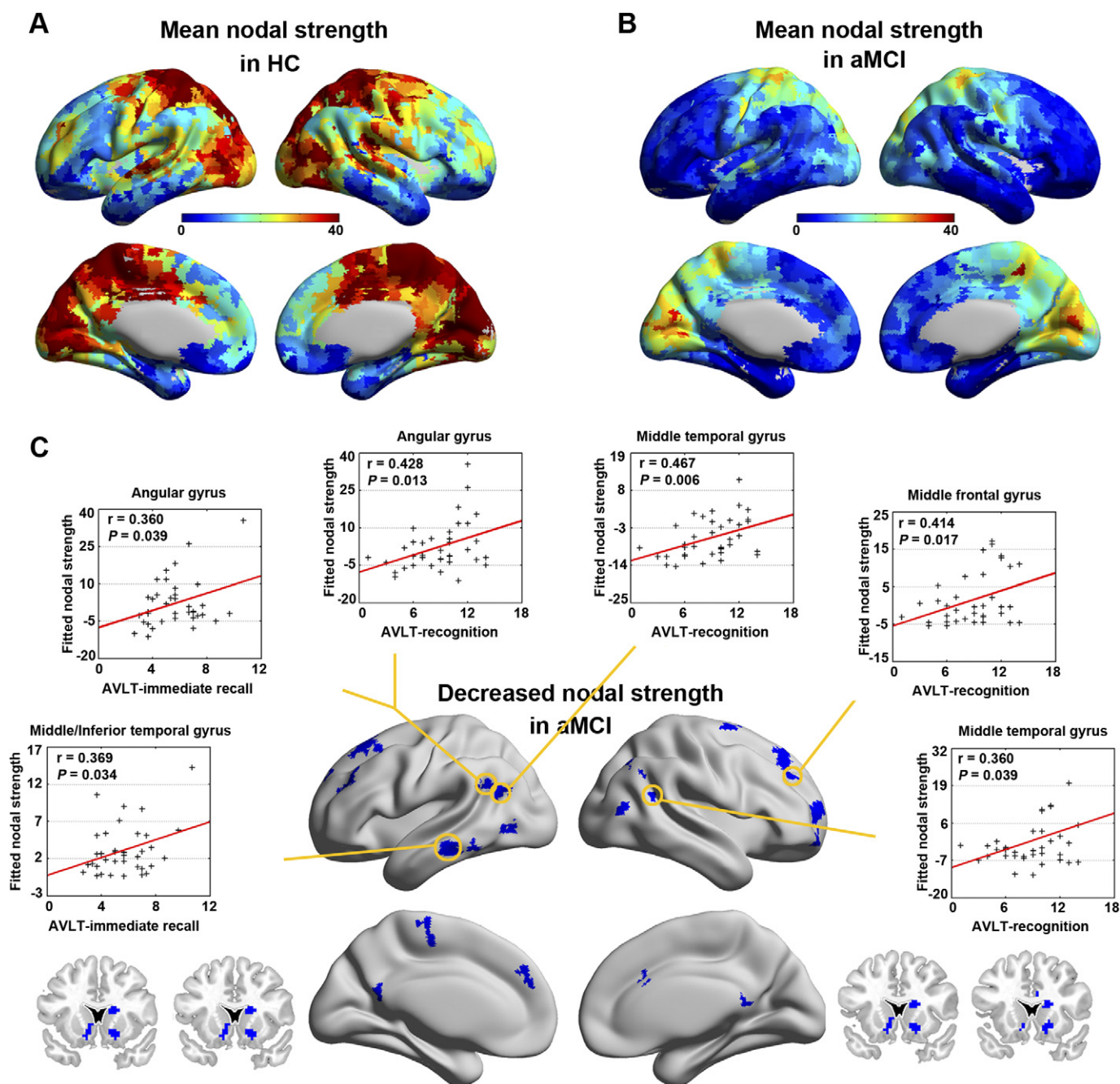


Figure 2. Mean nodal strength in the healthy control subjects (HC) (A) and amnesic mild cognitive impairment (aMCI) patients (B) and between-group differences (C). The nodes and connections were mapped onto the cortical surfaces using the BrainNet Viewer package (<http://www.nitrc.org/projects/bnv>). AVLT, Auditory Verbal Learning Test.

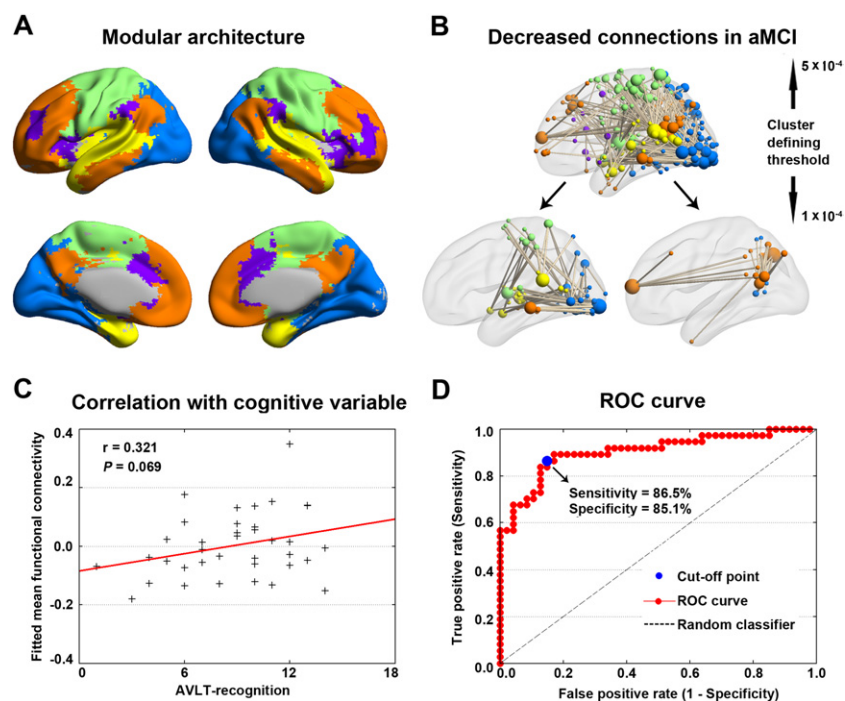


Figure 3. Modular architecture (A), amnesic mild cognitive impairment (aMCI)-related decrease in functional connectivity (B), connectivity-cognitive performance correlation (C), and aMCI-control classification (D). See Results for a description of these findings. AVLT, Auditory Verbal Learning Test; ROC, receiver operating characteristic.

structures were targeted ($p < .01$, uncorrected) by the disease that resided predominantly in the frontal (e.g., the bilateral dorsolateral superior frontal gyrus and middle frontal gyrus), parietal (e.g., the bilateral PCUN and angular gyrus), and temporal (e.g., the bilateral middle temporal gyrus [MTG] and left inferior temporal gyrus) regions (Figure 2C). In addition, several subcortical regions of the bilateral caudate nucleus and right putamen also showed decreased nodal strength in the aMCI patients (Figure 2C). We next considered the roles of these structures in the context of modular architecture derived from the HC group. Five modules were found ($Q_{\max} = .536$): the motor and somatosensory module, the default network, the (ventral) attention network, the visual processing module, and the auditory module (Figure 3A and Figure S1 in Supplement 1). Based on the identified modular architecture, the targeted ROIs in aMCI belonged mainly to the default network (19/27, 70.4%), followed by the attention (4/27, 14.8%), motor (2/27, 7.4%), and visual (2/27, 7.4%) modules.

Disrupted Functional Network Connectivity in aMCI

Under the cluster defining threshold of $p < 5 \times 10^{-4}$, a single network of 363 connections linking widely distributed brain structures was revealed to show decreased functional connectivity in the aMCI group ($p = .006$, corrected). Using a more rigorous threshold of $p < 1 \times 10^{-4}$, the network split into two independently connected components: one included 65 connections ($p = .004$, corrected) and the other 22 connections ($p = .011$, corrected). Using the normal modular architecture as a reference (Figure 3A), we

found that the larger component was comprised mainly of inter-module connections (46/65, 70.8%), which linked regions in the motor and somatosensory module, the visual processing module, and the auditory module (Figure 3B). In contrast, the smaller component was comprised predominantly of intramodule connections (15/22, 68.2%) within the default network (Figure 3B). These decreased functional connectivities were correlated significantly with the abnormal global network metrics mentioned above ($L^W: r = -.354, p = .001; \tilde{L}^W: r = -.574, p < 10^{-6}$).

Relationship Between Network Metrics and Behavioral Performance

Within the aMCI group, the whole-brain topology (L^W, \tilde{L}^W , and \tilde{Q}_{\max}) (Figure 4) and nodal strength (angular gyrus, MTG, inferior temporal gyrus, and middle frontal gyrus) (Figure 2C) correlated significantly ($p < .05$) with the AVLT-recognition and immediate recall ability of the patients (Table 2). Additionally, the mean functional connectivity strength of the NBS-based connected network (cluster-defining threshold, $p < 1 \times 10^{-4}$) exhibited a trend toward positive correlation with the AVLT-cognitive recognition (Figure 3C).

Sensitivity and Specificity of Network Metrics in Differentiating the aMCI Patients from HCs

The mean functional connectivity strength of the NBS-based connected network (cluster-defining threshold, $p < 1 \times 10^{-4}$) exhibited the highest power (area under curve = .904, $p < 10^{-6}$), with

Figure 4. The relationship between global network metrics and cognitive performance of patients with amnesic mild cognitive impairment. AVLT, Auditory Verbal Learning Test.

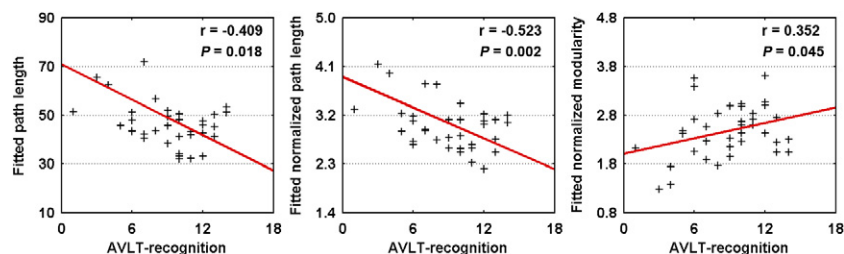


Table 2. Partial Correlation Coefficients Between Global and Nodal Network Metrics and Cognitive Performance of Patients with aMCI

Network Metric	Partial Correlation Coefficient (<i>p</i> Value)			
	MMSE	AVLT-Immediate Recall	AVLT-Delayed Recall	AVLT-Recognition
C^W	-.123 (.497)	.114 (.528)	-.044 (.809)	.348 (.048) ^a
L^W	.071 (.694)	-.207 (.247)	-.114 (.529)	-.409 (.018) ^a
Q_{max}	-.001 (.995)	-.214 (.232)	-.187 (.297)	-.446 (.009) ^a
\bar{C}^W	-.177 (.325)	-.300 (.089)	-.203 (.257)	-.455 (.008) ^a
\bar{L}^W	-.039 (.830)	-.232 (.194)	-.105 (.560)	-.523 (.002) ^a
\bar{Q}_{max}	-.003 (.989)	-.286 (.106)	-.038 (.835)	-.352 (.045) ^a
ANG, L	-.103 (.570)	-.360 (.39) ^a	-.205 (.253)	-.428 (.013) ^a
MTG, L/ITG, L	-.031 (.863)	-.369 (.035) ^a	-.222 (.214)	-.082 (.650)
MFG, R	-.028 (.878)	-.025 (.890)	-.016 (.929)	-.414 (.017) ^a
MTG, L	-.021 (.906)	-.214 (.231)	-.101 (.574)	-.467 (.006) ^a
MTG, R	-.096 (.594)	-.195 (.277)	-.147 (.413)	-.360 (.039) ^a

The partial correlations were computed using age, gender, the age-gender interaction, and education as confounding covariates.

aMCI, amnesic mild cognitive impairment; ANG, angular gyrus; AVLT, Auditory Verbal Learning Test; ITG, inferior temporal gyrus; L, left; MFG, middle frontal gyrus; MMSE, Mini-Mental State Examination; MTG, middle temporal gyrus; R, right.

^aSignificant (*p* < .05) correlations.

a sensitivity of 86.5% and a specificity of 85.1% (accuracy = 85.7%) for distinguishing patients from HCs (Figure 3D). As such, 32 out of the 37 patients with aMCI and 40 out of the 47 HCs were classified correctly. All of the other network metrics studied exhibited relatively poor discriminant performances (all areas under curve < .7).

Reproducibility of the Findings and Test-Retest Reliability of Wavelet-Derived Network Metrics

Most of the findings reported above were reproducible across different parcellation schemes (Table 3, Figures S2 and S3 in Supplement

1), preprocessing strategies and network types (data not shown). It should be noted that high-resolution parcellation outperformed low-resolution parcellation in discriminating patients with aMCI from HCs (Table 3). In the specific wavelet scale 3, most global wavelet-derived network metrics exhibited fair to excellent (.4 < intraclass correlation < .9) test-retest reliability (Figure S4 in Supplement 1), whereas the reliability of nodal strength distributed unequally across the brain (Figure S5 in Supplement 1). Notably, most of those metrics and brain structures that showed between-group differences exhibited moderate to high reliability.

Table 3. Reproducibility of Our Principal Findings Over Various Parcellation Schemes

Parcellation	C^W	L^W	Q_{max}	\bar{C}^W	\bar{L}^W	\bar{Q}_{max}	NBS
Between-Group Difference							
L-AAL (<i>n</i> = 90)	↓ ^a	↑ ^b	↑ ^b	ns	ns	ns	↓ ^a
L-HOA (<i>n</i> = 112)	↓ ^a	↑ ^b	↑ ^b	ns	ns	ns	↓ ^a
L-Crad (<i>n</i> = 200)	↓ ^a	ns	↑ ^b	ns	ns	↓ ^b	↓ ^a
H-1024 (<i>n</i> = 1024)	ns	↑ ^a	ns	ns	↑ ^b	↓ ^b	↓ ^a
Correlation Analysis							
L-AAL (<i>n</i> = 90)	+ ^a	- ^a	- ^a	- ^a	ns	+ ^b	ns
L-HOA (<i>n</i> = 112)	+ ^a	- ^a	- ^a	- ^a	- ^a	+ ^b	ns
L-Crad (<i>n</i> = 200)	+ ^b	- ^b	- ^a	- ^a	ns	+ ^b	ns
H-1024 (<i>n</i> = 1024)	+ ^a	- ^a	- ^a	- ^a	- ^a	+ ^a	+ ^b
Discriminant Analysis							
L-AAL (<i>n</i> = 90)	Poor	Poor	Poor	Poor	Poor	Poor	Fair
L-HOA (<i>n</i> = 112)	Poor	Poor	Poor	Poor	Poor	Poor	Good
L-Crad (<i>n</i> = 200)	Poor	Poor	Poor	Poor	Poor	Poor	Good
H-1024 (<i>n</i> = 1024)	Poor	Poor	Poor	Poor	Poor	Poor	Excellent

Correlations were significant only for AVLT-recognition. We did not describe the results of node analysis because of the incomparability across various parcellation schemes. All analyses were performed in wavelet scale 3 (.031–.063 Hz).

↓, aMCI < healthy control subjects; ↑, aMCI > healthy control subjects; +, positive correlation; -, negative correlation; AUC, area under curve; Excellent, AUC > 90%; Fair, 70% ≤ AUC < 80%; Good, 80% ≤ AUC < 90%; H-1024, high-resolution randomly generated atlas (38); L-AAL, low-resolution Anatomical Automatic Labeling atlas (100); L-Crad, Low-resolution Craddock *et al.* functional atlas (101); L-HOA, low-resolution Harvard-Oxford atlas (102,103); NBS, network-based statistic; the mean functional connectivity strength within the component identified using the network-based statistic method; ns, nonsignificant (*p* > .10); Poor, 60% ≤ AUC < 70%.

^a*p* < .05.

^b.05 ≤ *p* ≤ .10.

Discussion

We investigated the topological architecture of the functional connectome in patients with aMCI. We showed abnormal organization of the aMCI connectome from .031 Hz to .063 Hz, which was summarized as 1) an increased characteristic path length; 2) decreased nodal strength in the default network; and 3) impaired functional connectivity between different functional modules. Moreover, the abnormal network metrics correlated with patients' cognitive performance and distinguished patients from healthy elderly individuals with high sensitivity and specificity.

The human brain is a complex network that continuously integrates information across distributed brain regions. Recent studies have demonstrated that this powerful functionality has underlying substrates of nontrivial topological configuration, such as small-worldness and modularity. Within a network, small-worldness enables high efficiency of both specialized and integrated processing (41,55), and modularity enables faster adaptation by changing the functionality of one module without losing functionality in other modules (56). In this study, small-worldness and modularity were found in both the HC and aMCI groups, suggesting an optimal organization of the human brain to support efficient information transfer of both modular and distributed processing (57).

Despite the common functional architecture, quantitative analysis revealed a longer characteristic path length at a global level in patients with aMCI. A short path length ensures the effective integrity and rapid information propagation between and across remote regions of the brain that are believed to constitute the basis of cognitive processing (58). The aMCI-related increase may reflect disrupted neuronal integration between distant regions and is consistent with previous AD studies (20,21,23). However, a recent magnetoencephalography study reported a decreased path length in aMCI patients during a memory task (25). This discrepancy may be attributed to the different cognitive states (task vs. resting). During a memory task, aMCI patients may require more connections to achieve the same level of cognitive output (25), whereas during resting, the patients had fewer connections, which may reflect essential disconnections of spontaneous neural activity. Notably, using three low-resolution parcellation schemes, decreased clustering coefficients were also detected in the aMCI connectome, indicating a distinct specificity of different parcellation strategies in revealing the organization of the functional connectome.

Besides the global topologies, we also studied the node and connectivity attributes of the brain connectome. The posterior parietal and occipital cortex regions (e.g., the PCUN, postcentral gyrus, superior parietal gyrus, cuneus, and calcarine fissure and surrounding cortex) showed the highest nodal strength (i.e., hubs) in both the aMCI and HC groups, consistent with previous findings (43,59–61). Hub regions play pivotal roles in supporting high-level cognitive functions by coordinating the overall information flow and maintaining the integrity of the brain connectome. The similar hub distributions suggest a preservation of hubs in aMCI. Nevertheless, the patients showed decreased nodal strength in regions that reside predominantly in the default network (e.g., dorsolateral superior frontal gyrus, PCUN, and MTG). Previous studies have suggested that the default regions are structurally connected (62,63) and show coherent brain activity in both humans (64,65) and monkeys (66). These regions are involved primarily with episodic memory processes (64) and show a breakdown in spontaneous brain activity in mild cognitive impairment (MCI) (7,9,10,28). Thus, the decline of nodal strength in the default network is consistent with the previous studies and provides important implications for the

memory-related deficits in aMCI patients. Additionally, a few nodes in attention, motor, and visual modules also showed decreased nodal strength, indicating the impaired functioning in these domains as demonstrated in several previous studies (28,67–69).

Beyond the default network, the subcortical caudate and putamen also showed decreased nodal strength in patients with aMCI. The caudate and putamen are key nodes in the neostriatum; they receive numerous inputs from the cortex, send the connections to the basal ganglia nuclei, and then project back to the cortex via the thalamus (70,71). Several previous studies have shown that the caudate and putamen exhibit gray matter atrophy (72) and metabolic disruption (73) in patients with MCI. In the resting state, these structures also exhibited abnormal functional connectivity (28,74). These previous findings and our results provide evidence for both structural and functional MCI-related abnormalities in subcortical brain areas.

We identified a large, single disconnected network in the aMCI patients. This network comprised two components of connections linking different functional modules and connections within the single default network. This finding is comparable with previous reports of selected reductions of network-related activity in aMCI patients (7). Moreover, these connections were related directly to whole-brain network topology, suggesting their contribution to the observed global topological abnormalities. Therefore, it is reasonable to speculate that these disconnections led to decreased functional integration throughout the brain, which may further account for cognitive deficits in patients. Overall, our results provide empirical evidence for disrupted network organization in aMCI at three (global, nodal, and connectional) levels.

We found that the altered network metrics mentioned above correlated specifically with memory-related (AVLT) cognitive performance in patients with aMCI, indicating their potential in capturing the progress of aMCI. Notably, we did not detect significant correlations between network metrics and MMSE scores, which measure an overall cognitive performance covering multiple domains (30). Given the predominant cognitive deficits in memory function caused by aMCI, we speculate that the nonsignificant correlations between network metrics and MMSE could be obscured by other cognitive domains that are relatively preserved in aMCI.

Currently, the clinical diagnosis of aMCI has limited specificity and is prone to bias from subjective knowledge and experience. Therefore, an accurate and objective diagnosis of aMCI has high clinical value in preventing the progression to dementia. With this aim, previous studies have made great efforts to seek aMCI-related biomarkers by extracting regional features of cortical thickness (75,76), gray matter volume (76–78), white matter microstructure (79,80), and functional metabolism (81). More recently, researchers have moved beyond focal brain abnormalities to dysfunctional interregional connectivity for distinguishing aMCI from healthy control subjects (82–84). Using a receiver operating characteristic analysis, we showed that the NBS-based connectivity network differentiated aMCI patients from healthy individuals with high sensitivity and specificity. Interestingly, we noticed that connectivity strength outperformed both global and nodal network metrics in the aMCI classification. These data suggest that the measurement of connectivity is a preferential candidate for diagnosing aMCI. In the future, the ability to diagnose aMCI could be further improved by combining both structural and functional connectivity information from multimodality imaging data (68).

It is important to state that the disrupted functional connectome in patients with aMCI was detected exclusively in the specific frequency band of .031 Hz to .063 Hz. Previous studies have demonstrated the frequency specificity of the functional architecture of

the brain at multiple levels (36,85,86). Under clinical conditions, accumulating evidence also revealed frequency-dependent functional changes in the brain (33,37,87,88). These studies highlight the important role of frequency for brain functioning. Previous evidence indicates that neuronal oscillations are distributed linearly on the natural logarithmic scale and independent frequency bands are generated by distinct oscillators with specific properties and physiological functions (89,90). Higher frequency oscillations tend to be confined to small ensembles of neurons, whereas lower frequency oscillations allow for an integration of neuronal effects (89,90). Even within the same neuronal networks, neighboring bands are typically associated with different brain states and compete with each other (89,91). In this study, we detected aMCI-related alterations only in the .031 Hz to .063 Hz frequency interval, presumably as a consequence of impaired cognitive functioning in specific domains. However, it should be noted that the origins and mechanisms of the signals at different frequency bands remain largely unknown. Further studies are necessary to clarify these issues and to ascertain the underlying mechanisms of disease-frequency interactions.

Several issues need to be further addressed. First, mapping the brain connectome appropriately and precisely is a challenging task at the present time (92,93). We used a test-retest reliable wavelet-based approach and found reproducible aMCI-related changes across different parcellation schemes. Nevertheless, future studies employing other connectivity measures and parcellation schemes will provide more comprehensive insights into the aMCI connectome. Second, recent studies have shown significant effects of head motion on functional connectivity (94,95). Thus, we reanalyzed our data with head motion as an extra covariate in our statistical models and observed similar results (data not shown). Third, the nodal centrality results were not corrected by multiple comparisons; thus, this finding should be considered an exploratory analysis. Future studies are required to increase the statistical power with a larger sample size or by selecting ROIs relevant to aMCI a priori. Fourth, accumulating evidence suggests a shaping of structural pathways in functional networks (96,97). However, different topological features were observed between structural and functional brain networks (98). Thus, combining multimodal neuroimaging data will aid in uncovering structure-function relationships in aMCI patients. Fifth, aMCI patients exhibit different progressive trajectories, where some ultimately develop AD and others do not. Accordingly, follow-up longitudinal connectome-based studies are warranted to elucidate the underlying mechanism that contributes to these disparate disease trajectories. Finally, beyond the aMCI studied here, there are other high-risk factors for developing AD, such as genetic risk of apolipoprotein (APOE) ϵ 4 allele. A recent diffusion tensor imaging study has shown that the structural connectome in aging is mediated by APOE ϵ 4 (99). However, the whole-brain functional connectome has been not studied in APOE ϵ 4 carriers, which would be an interesting topic for the future.

This work was supported by the Natural Science Foundation of China (Grant numbers 81030028, 30970823, and 81171409), Beijing Natural Science Foundation (Grant number 7102090, Z111107067311036), and the Startup Foundation for Distinguished Research Professor of Institute of Psychology, Chinese Academy of Sciences (Y0CX492503, XNZ).

We thank Dr. R. Cameron Craddock for kindly providing functionally defined regions and Dr. Andrew Zalesky for kindly providing codes to generate high-resolution parcellation atlas.

The authors report no biomedical financial interests or potential conflicts of interest.

Supplementary material cited in this article is available online.

1. Delbeuck X, Van der Linden M, Collette F (2003): Alzheimer' disease as a disconnection syndrome? *Neuropsychol Rev* 13:79–92.
2. He Y, Chen Z, Gong G, Evans A (2009): Neuronal networks in Alzheimer's disease. *Neuroscientist* 15:333–350.
3. Filippi M, Agosta F (2011): Structural and functional network connectivity breakdown in Alzheimer's disease studied with magnetic resonance imaging techniques. *J Alzheimers Dis* 24:455–474.
4. Petersen RC, Smith GE, Waring SC, Ivnik RJ, Tangalos EG, Kokmen E (1999): Mild cognitive impairment: Clinical characterization and outcome. *Arch Neurol* 56:303–308.
5. Choo IH, Lee DY, Oh JS, Lee JS, Lee DS, Song IC, *et al.* (2010): Posterior cingulate cortex atrophy and regional cingulum disruption in mild cognitive impairment and Alzheimer's disease. *Neurobiol Aging* 31:772–779.
6. Zhuang L, Wen W, Zhu W, Trollor J, Kochan N, Crawford J, *et al.* (2010): White matter integrity in mild cognitive impairment: A tract-based spatial statistics study. *Neuroimage* 53:16–25.
7. Sorg C, Riedl V, Muhlau M, Calhoun VD, Eichele T, Laer L, *et al.* (2007): Selective changes of resting-state networks in individuals at risk for Alzheimer's disease. *Proc Natl Acad Sci U S A* 104:18760–18765.
8. Bai F, Zhang Z, Watson DR, Yu H, Shi Y, Yuan Y, *et al.* (2009): Abnormal functional connectivity of hippocampus during episodic memory retrieval processing network in amnesic mild cognitive impairment. *Biol Psychiatry* 65:951–958.
9. Drzezga A, Becker JA, Van Dijk KR, Sreenivasan A, Talukdar T, Sullivan C, *et al.* (2011): Neuronal dysfunction and disconnection of cortical hubs in non-demented subjects with elevated amyloid burden. *Brain* 134:1635–1646.
10. Petrella JR, Sheldon FC, Prince SE, Calhoun VD, Doraiswamy PM (2011): Default mode network connectivity in stable vs progressive mild cognitive impairment. *Neurology* 76:511–517.
11. Sporns O, Tononi G, Kotter R (2005): The human connectome: A structural description of the human brain. *PLoS Comput Biol* 1:e42.
12. Biswal BB, Mennes M, Zuo XN, Gohel S, Kelly C, Smith SM, *et al.* (2010): Toward discovery science of human brain function. *Proc Natl Acad Sci U S A* 107:4734–4739.
13. Bullmore E, Sporns O (2009): Complex brain networks: Graph theoretical analysis of structural and functional systems. *Nat Rev Neurosci* 10:186–198.
14. Sporns O (2011): The human connectome: A complex network. *Ann NY Acad Sci* 1224:109–125.
15. He Y, Evans A (2010): Graph theoretical modeling of brain connectivity. *Curr Opin Neurol* 23:341–350.
16. Bassett DS, Bullmore ET (2009): Human brain networks in health and disease. *Curr Opin Neurol* 22:340–347.
17. Guye M, Bettus G, Bartolomei F, Cozzone PJ (2010): Graph theoretical analysis of structural and functional connectivity MRI in normal and pathological brain networks. *MAGMA* 23:409–421.
18. Xia M, He Y (2011): Magnetic resonance imaging and graph theoretical analysis of complex brain networks in neuropsychiatric disorders. *Brain Connect* 1:349–365.
19. Stam CJ, de Haan W, Daffertshofer A, Jones BF, Manshanden I, van Cappellen van Walsum AM, *et al.* (2009): Graph theoretical analysis of magnetoencephalographic functional connectivity in Alzheimer's disease. *Brain* 132:213–224.
20. Stam CJ, Jones BF, Nolte G, Breakspear M, Scheltens P (2007): Small-world networks and functional connectivity in Alzheimer's disease. *Cereb Cortex* 17:92–99.
21. He Y, Chen Z, Evans A (2008): Structural insights into aberrant topological patterns of large-scale cortical networks in Alzheimer's disease. *J Neurosci* 28:4756–4766.
22. Supekar K, Menon V, Rubin D, Musen M, Greicius MD (2008): Network analysis of intrinsic functional brain connectivity in Alzheimer's disease. *PLoS Comput Biol* 4:e1000100.
23. Lo CY, Wang PN, Chou KH, Wang J, He Y, Lin CP (2010): Diffusion tensor tractography reveals abnormal topological organization in structural cortical networks in Alzheimer's disease. *J Neurosci* 30:16876–16885.
24. Yao Z, Zhang Y, Lin L, Zhou Y, Xu C, Jiang T (2010): Abnormal cortical networks in mild cognitive impairment and Alzheimer's disease. *PLoS Comput Biol* 6:e1001006.

25. Buldu JM, Bajo R, Maestu F, Castellanos N, Leyva I, Gil P, *et al.* (2011): Reorganization of functional networks in mild cognitive impairment. *PLoS One* 6:e19584.
26. Biswal B, Yetkin FZ, Haughton VM, Hyde JS (1995): Functional connectivity in the motor cortex of resting human brain using echo-planar MRI. *Magn Reson Med* 34:537–541.
27. Fox MD, Raichle ME (2007): Spontaneous fluctuations in brain activity observed with functional magnetic resonance imaging. *Nat Rev Neurosci* 8:700–711.
28. Bai F, Liao W, Watson DR, Shi Y, Wang Y, Yue C, *et al.* (2011): Abnormal whole-brain functional connection in amnesic mild cognitive impairment patients. *Behav Brain Res* 216:666–672.
29. Petersen RC, Stevens JC, Ganguli M, Tangalos EG, Cummings JL, DeKosky ST (2001): Practice parameter: Early detection of dementia: Mild cognitive impairment (an evidence-based review). Report of the Quality Standards Subcommittee of the American Academy of Neurology. *Neurology* 56:1133–1142.
30. Folstein MF, Folstein SE, McHugh PR (1975): “Mini-mental state”: A practical method for grading the cognitive state of patients for the clinician. *J Psychiatr Res* 12:189–198.
31. Morris JC (1993): The Clinical Dementia Rating (CDR): Current version and scoring rules. *Neurology* 43:2412–2414.
32. Maj M, D’Elia L, Satz P, Janssen R, Zaudig M, Uchiyama C, *et al.* (1993): Evaluation of two new neuropsychological tests designed to minimize cultural bias in the assessment of HIV-1 seropositive persons: A WHO study. *Arch Clin Neuropsychol* 8:123–135.
33. Han Y, Wang J, Zhao Z, Min B, Lu J, Li K, *et al.* (2011): Frequency-dependent changes in the amplitude of low-frequency fluctuations in amnesic mild cognitive impairment: A resting-state fMRI study. *Neuroimage* 55:287–295.
34. Fox MD, Zhang D, Snyder AZ, Raichle ME (2009): The global signal and observed anticorrelated resting state brain networks. *J Neurophysiol* 101:3270–3283.
35. Murphy K, Birn RM, Handwerker DA, Jones TB, Bandettini PA (2009): The impact of global signal regression on resting state correlations: Are anti-correlated networks introduced? *Neuroimage* 44:893–905.
36. Achard S, Salvador R, Whitcher B, Suckling J, Bullmore E (2006): A resilient, low-frequency, small-world human brain functional network with highly connected association cortical hubs. *J Neurosci* 26:63–72.
37. Lynall ME, Bassett DS, Kerwin R, McKenna PJ, Kitzbichler M, Muller U, Bullmore E (2010): Functional connectivity and brain networks in schizophrenia. *J Neurosci* 30:9477–9487.
38. Zalesky A, Fornito A, Harding IH, Cocchi L, Yucel M, Pantelis C, Bullmore E (2010): Whole-brain anatomical networks: Does the choice of nodes matter? *Neuroimage* 50:970–983.
39. Percival DB, Walden AT (2000): *Wavelet Methods for Time Series Analysis*. Cambridge, UK: Cambridge University Press.
40. Bassett DS, Wymbs NF, Porter MA, Mucha PJ, Carlson JM, Grafton ST (2011): Dynamic reconfiguration of human brain networks during learning. *Proc Natl Acad Sci U S A* 108:7641–7646.
41. Watts DJ, Strogatz SH (1998): Collective dynamics of ‘small-world’ networks. *Nature* 393:440–442.
42. Newman MEJ (2006): Finding community structure in networks using the eigenvectors of matrices. *Phys Rev E* 74:036104.
43. Zuo XN, Ehmke R, Mennes M, Imperati D, Castellanos FX, Sporns O, Milham MP (2011): Network centrality in the human functional connectome [published online ahead of print October 12]. *Cereb Cortex*. doi: 10.1093/cercor/bhr269.
44. Wang JH, Zuo XN, Gohel S, Milham MP, Biswal BB, He Y (2011): Graph theoretical analysis of functional brain networks: Test-retest evaluation on short- and long-term resting-state functional MRI data. *PLoS One* 6:e21976.
45. Rubinov M, Sporns O (2010): Complex network measures of brain connectivity: Uses and interpretations. *Neuroimage* 52:1059–1069.
46. Bullmore ET, Suckling J, Overmeyer S, Rabe-Hesketh S, Taylor E, Brammer MJ (1999): Global, voxel, and cluster tests, by theory and permutation, for a difference between two groups of structural MR images of the brain. *IEEE Trans Med Imaging* 18:32–42.
47. Zalesky A, Fornito A, Bullmore ET (2010): Network-based statistic: Identifying differences in brain networks. *Neuroimage* 53:1197–1207.
48. Gong G, Rosa-Neto P, Carbonell F, Chen ZJ, He Y, Evans AC (2009): Age- and gender-related differences in the cortical anatomical network. *J Neurosci* 29:15684–15693.
49. Zhu W, Wen W, He Y, Xia A, Anstey KJ, Sachdev P (2012): Changing topological patterns in normal aging using large-scale structural networks. *Neurobiol Aging* 33:899–913.
50. Wang L, Li Y, Metzack P, He Y, Woodward TS (2010): Age-related changes in topological patterns of large-scale brain functional networks during memory encoding and recognition. *Neuroimage* 50:862–872.
51. Tian L, Wang J, Yan C, He Y (2011): Hemisphere- and gender-related differences in small-world brain networks: A resting-state functional MRI study. *Neuroimage* 54:191–202.
52. Yan C, Gong G, Wang J, Wang D, Liu D, Zhu C, *et al.* (2011): Sex- and brain size-related small-world structural cortical networks in young adults: A DTI tractography study. *Cereb Cortex* 21:449–458.
53. Micheloyannis S, Pachou E, Stam CJ, Vourkas M, Erimaki S, Tsirka V (2006): Using graph theoretical analysis of multi channel EEG to evaluate the neural efficiency hypothesis. *Neurosci Lett* 402:273–277.
54. Shrout PE, Fleiss JL (1979): Intraclass correlations: Uses in assessing rater reliability. *Psychol Bull* 86:420–428.
55. Latora V, Marchiori M (2003): Economic small-world behavior in weighted networks. *Eur Phys J B* 32:249–263.
56. Simon HA (1962): The architecture of complexity. *Proc Am Philos Soc* 106:467–482.
57. Wang J, Zuo X, He Y (2010): Graph-based network analysis of resting-state functional MRI. *Front Syst Neurosci* 4:16.
58. Sporns O, Zwi JD (2004): The small world of the cerebral cortex. *Neuroinformatics* 2:145–162.
59. Hagmann P, Cammoun L, Gigandet X, Meuli R, Honey CJ, Wedeen VJ, Sporns O (2008): Mapping the structural core of human cerebral cortex. *PLoS Biol* 6:e159.
60. Buckner RL, Sepulcre J, Talukdar T, Krienen FM, Liu H, Hedden T, *et al.* (2009): Cortical hubs revealed by intrinsic functional connectivity: Mapping, assessment of stability, and relation to Alzheimer’s disease. *J Neurosci* 29:1860–1873.
61. Tomasi D, Volkow ND (2010): Functional connectivity density mapping. *Proc Natl Acad Sci U S A* 107:9885–9890.
62. Greicius MD, Supekar K, Menon V, Dougherty RF (2009): Resting-state functional connectivity reflects structural connectivity in the default mode network. *Cereb Cortex* 19:72–78.
63. Teipel SJ, Bokde AL, Meindl T, Amaro E Jr, Soldner J, Reiser MF, *et al.* (2010): White matter microstructure underlying default mode network connectivity in the human brain. *Neuroimage* 49:2021–2032.
64. Greicius MD, Krasnow B, Reiss AL, Menon V (2003): Functional connectivity in the resting brain: A network analysis of the default mode hypothesis. *Proc Natl Acad Sci U S A* 100:253–258.
65. Fox MD, Snyder AZ, Vincent JL, Corbetta M, Van Essen DC, Raichle ME (2005): The human brain is intrinsically organized into dynamic, anticorrelated functional networks. *Proc Natl Acad Sci U S A* 102:9673–9678.
66. Vincent JL, Patel GH, Fox MD, Snyder AZ, Baker JT, Van Essen DC, *et al.* (2007): Intrinsic functional architecture in the anaesthetized monkey brain. *Nature* 447:83–86.
67. Wang Z, Jia X, Liang P, Qi Z, Yang Y, Zhou W, Li K (2011): Changes in thalamus connectivity in mild cognitive impairment: Evidence from resting state fMRI. *Eur J Radiol* 3575–3575.
68. Wee CY, Yap PT, Zhang D, Denny K, Browndyke JN, Potter GG, *et al.* (2012): Identification of MCI individuals using structural and functional connectivity networks. *Neuroimage* 59:2045–2056.
69. Aggarwal NT, Wilson RS, Beck TL, Bienias JL, Bennett DA (2006): Motor dysfunction in mild cognitive impairment and the risk of incident Alzheimer disease. *Arch Neurol* 63:1763–1769.
70. Alexander GE, DeLong MR, Strick PL (1986): Parallel organization of functionally segregated circuits linking basal ganglia and cortex. *Annu Rev Neurosci* 9:357–381.
71. Postuma RB, Dagher A (2006): Basal ganglia functional connectivity based on a meta-analysis of 126 positron emission tomography and functional magnetic resonance imaging publications. *Cereb Cortex* 16: 1508–1521.
72. Madsen SK, Ho AJ, Hua X, Saharan PS, Toga AW, Jack CR Jr, *et al.* (2010): 3D maps localize caudate nucleus atrophy in 400 Alzheimer’s disease, mild cognitive impairment, and healthy elderly subjects. *Neurobiol Aging* 31:1312–1325.
73. Koivunen J, Scheinin N, Virta JR, Aalto S, Vahlberg T, Nagren K, *et al.* (2011): Amyloid PET imaging in patients with mild cognitive impairment: A 2-year follow-up study. *Neurology* 76:1085–1090.

74. Liang P, Wang Z, Yang Y, Jia X, Li K (2011): Functional disconnection and compensation in mild cognitive impairment: Evidence from DLPFC connectivity using resting-state fMRI. *PLoS One* 6:e22153.
75. Querbes O, Aubry F, Pariente J, Lotterie JA, Demonet JF, Duret V, *et al.* (2009): Early diagnosis of Alzheimer's disease using cortical thickness: Impact of cognitive reserve. *Brain* 132:2036–2047.
76. Desikan RS, Cabral HJ, Hess CP, Dillon WP, Glastonbury CM, Weiner MW, *et al.* (2009): Automated MRI measures identify individuals with mild cognitive impairment and Alzheimer's disease. *Brain* 132:2048–2057.
77. Colliot O, Chetelat G, Chupin M, Desgranges B, Magnin B, Benali H, *et al.* (2008): Discrimination between Alzheimer disease, mild cognitive impairment, and normal aging by using automated segmentation of the hippocampus. *Radiology* 248:194–201.
78. Westman E, Simmons A, Zhang Y, Muehlboeck JS, Tunnard C, Liu Y, *et al.* (2011): Multivariate analysis of MRI data for Alzheimer's disease, mild cognitive impairment and healthy controls. *Neuroimage* 54:1178–1187.
79. Muller MJ, Greverus D, Weibrich C, Dellani PR, Scheurich A, Stoeter P, Fellgiebel A (2007): Diagnostic utility of hippocampal size and mean diffusivity in amnesic MCI. *Neurobiol Aging* 28:398–403.
80. Haller S, Nguyen D, Rodriguez C, Emch J, Gold G, Bartsch A, *et al.* (2010): Individual prediction of cognitive decline in mild cognitive impairment using support vector machine-based analysis of diffusion tensor imaging data. *J Alzheimers Dis* 22:315–327.
81. De Santi S, de Leon MJ, Rusinek H, Convit A, Tarshish CY, Roche A, *et al.* (2001): Hippocampal formation glucose metabolism and volume losses in MCI and AD. *Neurobiol Aging* 22:529–539.
82. Wee CY, Yap PT, Li W, Denny K, Browndyke JN, Potter GG, *et al.* (2011): Enriched white matter connectivity networks for accurate identification of MCI patients. *Neuroimage* 54:1812–1822.
83. Zhou L, Wang Y, Li Y, Yap PT, Shen D (2011): Hierarchical anatomical brain networks for MCI prediction: Revisiting volumetric measures. *PLoS One* 6:e21935.
84. Chen G, Ward BD, Xie C, Li W, Wu Z, Jones JL, *et al.* (2011): Classification of Alzheimer disease, mild cognitive impairment, and normal cognitive status with large-scale network analysis based on resting-state functional MR imaging. *Radiology* 259:213–221.
85. Salvador R, Martinez A, Pomarol-Clotet E, Gomar J, Vila F, Sarro S, *et al.* (2008): A simple view of the brain through a frequency-specific functional connectivity measure. *Neuroimage* 39:279–289.
86. Zuo XN, Di Martino A, Kelly C, Shehzad ZE, Gee DG, Klein DF, *et al.* (2010): The oscillating brain: Complex and reliable. *Neuroimage* 49:1432–1445.
87. Di Martino A, Ross K, Uddin LQ, Sklar AB, Castellanos FX, Milham MP (2009): Functional brain correlates of social and nonsocial processes in autism spectrum disorders: An activation likelihood estimation meta-analysis. *Biol Psychiatry* 65:63–74.
88. Hoptman MJ, Zuo X-N, Butler PD, Javitt DC, D'Angelo D, Mauro CJ, Milham MP (2010): Amplitude of low-frequency oscillations in schizophrenia: A resting state fMRI study. *Schizophr Res* 117:13–20.
89. Buzsaki G, Geisler C, Henze DA, Wang X-J (2004): Interneuron Diversity series: Circuit complexity and axon wiring economy of cortical interneurons. *Trends Neurosci* 27:186–193.
90. Penttonen M (2003): Natural logarithmic relationship between brain oscillators. *Thal Relat Syst* 2:145–152.
91. Engel AK, Fries P, Singer W (2001): Dynamic predictions: Oscillations and synchrony in top-down processing. *Nat Rev Neurosci* 2:704–716.
92. Butts CT (2009): Revisiting the foundations of network analysis. *Science* 325:414–416.
93. Smith SM, Miller KL, Salimi-Khorshidi G, Webster M, Beckmann CF, Nichols TE, *et al.* (2011): Network modelling methods for FMRI. *Neuroimage* 54:875–891.
94. Van Dijk KR, Sabuncu MR, Buckner RL (2012): The influence of head motion on intrinsic functional connectivity MRI. *Neuroimage* 59:431–438.
95. Power JD, Barnes KA, Snyder AZ, Schlaggar BL, Petersen SE (2012): Spurious but systematic correlations in functional connectivity MRI networks arise from subject motion. *Neuroimage* 59:2142–2154.
96. Honey CJ, Sporns O, Cammoun L, Gigandet X, Thiran JP, Meuli R, Hagmann P (2009): Predicting human resting-state functional connectivity from structural connectivity. *Proc Natl Acad Sci U S A* 106:2035–2040.
97. van den Heuvel MP, Mandl RC, Kahn RS, Hulshoff Pol HE (2009): Functionally linked resting-state networks reflect the underlying structural connectivity architecture of the human brain. *Hum Brain Mapp* 30:3127–3141.
98. Park C-h, Kim SY, Kim Y-H, Kim K (2008): Comparison of the small-world topology between anatomical and functional connectivity in the human brain. *Physica A* 387:5958–5962.
99. Brown JA, Terashima KH, Burggren AC, Ercoli LM, Miller KJ, Small GW, Bookheimer SY (2011): Brain network local interconnectivity loss in aging APOE-4 allele carriers. *Proc Natl Acad Sci U S A* 108:20760–20765.
100. Tzourio-Mazoyer N, Landeau B, Papathanassiou D, Crivello F, Etard O, Delcroix N, *et al.* (2002): Automated anatomical labeling of activations in SPM using a macroscopic anatomical parcellation of the MNI MRI single-subject brain. *Neuroimage* 15:273–289.
101. Craddock RC, James GA, Holtzheimer PE 3rd, Hu XP, Mayberg HS (2011): A whole brain fMRI atlas generated via spatially constrained spectral clustering [published online ahead of print July 18]. *Hum Brain Mapp*. doi:10.1002/hbm.21333.
102. Kennedy DN, Lange N, Makris N, Bates J, Meyer J, Caviness VS, Jr. (1998): Gyri of the human neocortex: an MRI-based analysis of volume and variance. *Cereb Cortex* 8:372–384.
103. Makris N, Meyer JW, Bates JF, Yeterian EH, Kennedy DN, Caviness VS (1999): MRI-Based topographic parcellation of human cerebral white matter and nuclei II. Rationale and applications with systematics of cerebral connectivity. *Neuroimage* 9:18–45.